Biophysical Letter

Action Potential Morphology of Human Induced Pluripotent Stem Cell-Derived Cardiomyocytes Does Not Predict Cardiac Chamber Specificity and Is Dependent on Cell Density

David T. M. Du,[1] Nicola Hellen,[1] Christopher Kane,[1] and Cesare M. N. Terracciano[1,*]
[1]Myocardial Function Section, National Heart and Lung Institute, Imperial Centre for Translational and Experimental Medicine, Imperial College London, London, United Kingdom

ABSTRACT Previous studies investigating human induced pluripotent stem cell-derived cardiomyocytes (iPSC-CMs) have proposed the distinction of heart chamber-specific (atrial, ventricular, pacemaker) electrophysiological phenotypes based on action potential (AP) morphology. This suggestion has been based on data acquired using techniques that allow measurements from only a small number of cells and at low seeding densities. It has also been observed that density of culture affects the properties of iPSC-CMs. Here we systematically analyze AP morphology from iPSC-CMs at two seeding densities: 60,000 cells/well (confluent monolayer) and 15,000 cells/well (sparsely-seeded) using a noninvasive optical method. The confluent cells ($n = 360$) demonstrate a series of AP morphologies on a normally distributed spectrum with no evidence for specific subpopulations. The AP morphologies of sparsely seeded cells ($n = 32$) displayed a significantly different distribution, but even in this case there is no clear evidence of chamber-specificity. Reduction in gap junction conductance using carbenoxolone only minimally affected APD distribution in confluent cells. These data suggest that iPSC-CMs possess a *sui generis* AP morphology, and when observed in different seeding densities may encompass any shape including those resembling chamber-specific subtypes. These results may be explained by different functional maturation due to culture conditions.

Received for publication 18 June 2014 and in final form 3 November 2014.

*Correspondence: c.terracciano@imperial.ac.uk

Terminally differentiated atrial, ventricular, and nodal cardiomyocytes possess distinct electrophysiological properties. Earlier studies investigating human induced pluripotent stem cell-derived cardiomyocytes (iPSC-CMs) have proposed the distinction of heart chamber-specific (atrial, ventricular, pacemaker) electrophysiological phenotypes based on action potential (AP) morphology (1–9), and there have been major efforts to develop methods to purify iPSC-CMs to differentiate with such specificity (1,2,8). Electrophysiological studies of iPSC-CMs have reported cardiac chamber-specific differentiation among proprietary cardiac cell lines (6). The ability to discriminate stem cell-derived cardiomyocytes with higher degrees of specificity would prove a major development for the modeling of cardiac diseases such as long-QT syndrome, and cardiac tissue regeneration (1–10). There have also been a number of electrophysiological studies attempting to determine chamber-specific phenotypes of human embryonic stem cell-derived cardiomyocytes (10). The majority of these studies have used qualitative criteria to classify electrophysiological phenotypes. Due to the lack of very specific chamber-specific markers, quantitative determination of chamber-specific phenotypes has relied on analysis of the AP. Parameters include APD_{90}, APD_{50} (time taken to reach 90% and 50% repolarization, respectively), time to peak, and rate of depolarization among others. Previous electrophysiological studies assessing the chamber-specificity of iPSC-CMs have used low-throughput patch-clamping and microelectrode techniques, requiring the use of isolated cells.

However, cells seeded at low density often show substantial variability in morphology and function and a systematic study on confluent monolayers of iPSC-CMs is lacking. Optical mapping is an ideal technique for these studies, inasmuch as it allows measuring of AP morphology from a large number of cells simultaneously and noninvasively. However, where optical methods of measuring APs were used, only embryoid bodies were assessed (2). The extent to which seeding density affects AP morphology of iPSC-CMs is currently unknown, raising concerns over the relevance of these previous findings. In an attempt to explore the effects of seeding density on the differentiation in chamber-specific phenotypes, we systematically analyzed AP morphology of large samples of iPSC-CMs at both high- and low-seeding densities, using a medium throughput noninvasive optical technique (Fig. 1 *A* and Supporting Materials and Methods in the Supporting Material). Data are expressed as mean (standard deviation).

Editor: Godfrey Smith.

http://dx.doi.org/10.1016/j.bpj.2014.11.008

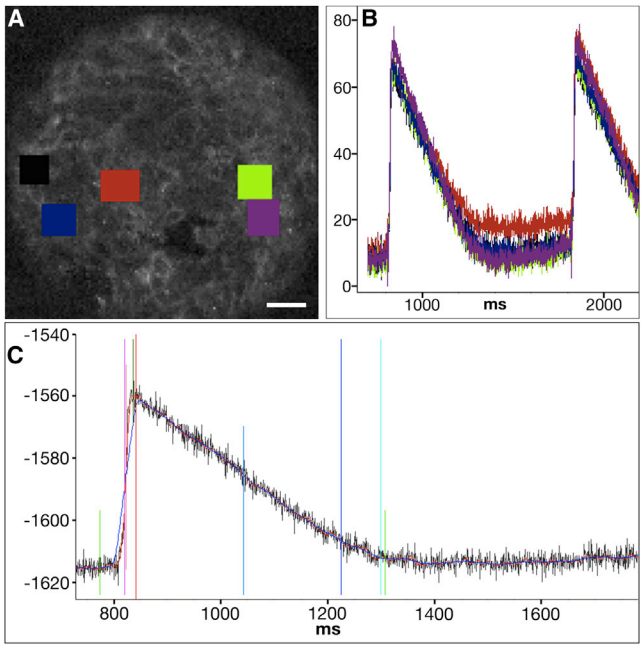

FIGURE 1 Optical measurement of human iPSC-CM transmembrane potential and analysis of AP parameter data. (*A*) Image of a selection of iPSC-CMs in a confluent monolayer at ×40 magnification. Cells in both seeding groups were stained with di-8-ANEPPS and field-stimulated at 1 Hz, allowing similar visualization. (*B*) Multiple APs of the corresponding iPSC-CM selections generated over time. (*C*) Single AP viewed in expanded timescale in analysis software, OPTIQ (Dr Francis Burton, University of Glasgow, Glasgow, UK). Curve-fitting and AP parameters were identified using OPTIQ. Vertical marks: (*red*) operator-selected peak amplitude; (*dark green*) OPTIQ-selected peak amplitude; (*purple*) maximum *dV/dt*; (*blue*) APD_{50}; (*dark blue*) APD_{90}; (*turquoise*) time at which repolarization ends; and (*green*) estimated time AP returns to baseline. Vertical axes are arbitrary units. Scale bar, 50 μm.

iPSC-CMs in the sparsely seeded group largely demonstrated longer APs with greater heterogeneity than the confluent group (confluent APD_{90}, 477.4 (66.8) ms, $n = 360$; sparse APD_{90}, 534.6 (128) ms, $n = 32$; F-statistic = 3.667, $p < 0.001$; see Fig. 2 *A*). We calculated goodness-of-fit to the Gaussian curve working on the assumption that a high goodness-of-fit indicates a low chance of three chamber subpopulations being present. APD_{90} from confluent cells displayed a high goodness-of-fit ($R^2 = 0.916$); sparsely seeded cells showed a poor goodness-of-fit ($R^2 = 0.583$; see Fig. 2 *A*). The lower goodness-of-fit in sparsely seeded cells can also be explained by the lower ($n = 32$) number of cells used, typically in the range of patch-clamping studies (1,3,4,6–9). Differences in distribution were statistically significant (K-S test, $p < 0.001$; see Fig. 2 *B*).

Time in repolarization (calculated as $APD_{90} - APD_{50}$) of the sparse cells demonstrated greater heterogeneity and the variance was significantly different to confluent cells (confluent, 181.8 (30.3) ms, $n = 360$; sparse, 203.1 (77) ms, $n = 32$; F-statistic = 6.453, $p < 0.001$; see Fig. 2 *C*). Sparse cells showed a poor fit to the Gaussian curve compared to confluent (confluent $R^2 = 0.939$; sparse $R^2 = 0.759$), and the distribution was significantly different to that of confluent cells (K-S test, $p < 0.01$; see Fig. 2 *D*).

We plotted the fraction in repolarization of cells in both seeding groups (calculated as $(APD_{90} - APD_{50})/APD_{90}$; see Fig. 2 *E*). Sparse cells, again, demonstrated a more heterogeneous distribution and a significantly different variance (confluent, 0.384 (0.06), $n = 360$; sparse, 0.386 (0.12), $n = 32$; F-statistic = 3.433, $p < 0.001$). Sparse cells demonstrated a poor fit to Gaussian curve (confluent $R^2 = 0.982$, sparse $R^2 = 0.673$), and distributions of fraction in repolarization between both seeding groups were significantly different (K-S test, $p < 0.05$; see Fig. 2 *F*).

Linear regression analysis of APD_{90} against time in repolarization revealed a positive correlation for both confluent and sparse cells (Fig. 2 *G*). APD_{90} plotted against fraction in repolarization revealed a negative correlation (Fig. 2 *H*). Working on the assumption that the relation between APD and repolarization time is distinctive for a specific chamber (i.e., atrial cells having a shorter, more triangular AP and ventricular cells having a longer AP that repolarizes faster), we would expect an unequivocal linear correlation between both APD with repolarization time, and APD with fraction in repolarization, with clustering of data around the most common morphologies for each chamber. However, this correlation is small in the confluent cells and is less evident in the sparsely seeded group. In addition, it is not possible to define any boundary in the data that allows ascribing an AP to a specific chamber.

To avoid the possibility that, in the confluent group, intercellular communication reduces variability of APD in adjacent cells, we reduced gap junction conductance using 20 μM carbenoxolone (11) (see the Supporting Materials and Methods in the Supporting Material). This did not affect mean APD, and despite an increase in variability of APD_{90} in these densely seeded cells (baseline, 505.7 (22.9) ms, $n = 112$; carbenoxolone, 509.5 (29.9) ms, $n = 133$; t-test, $p > 0.05$; F-statistic = 1.703, $p < 0.01$; see Fig. 3, *A* and *B*), this increase was small compared to the sparse cells (carbenoxolone F-statistic = 1.703; sparse F-statistic = 3.667). This suggests the greater variance seen in the sparse cell density cultures was predominantly due to the effects of seeding density itself, rather than the more limited intercellular connectivity between adjacent cells.

The two main findings of this study are as follows.

1. Seeding density significantly affects AP morphology. A different degree of electrical communication explains only a fraction of this effect and more studies are required to understand the mechanisms involved in the culture-dependent effects.
2. Cells from both seeding density groups demonstrate a series of AP morphologies on a normally distributed spectrum with no evidence for specific subpopulations.

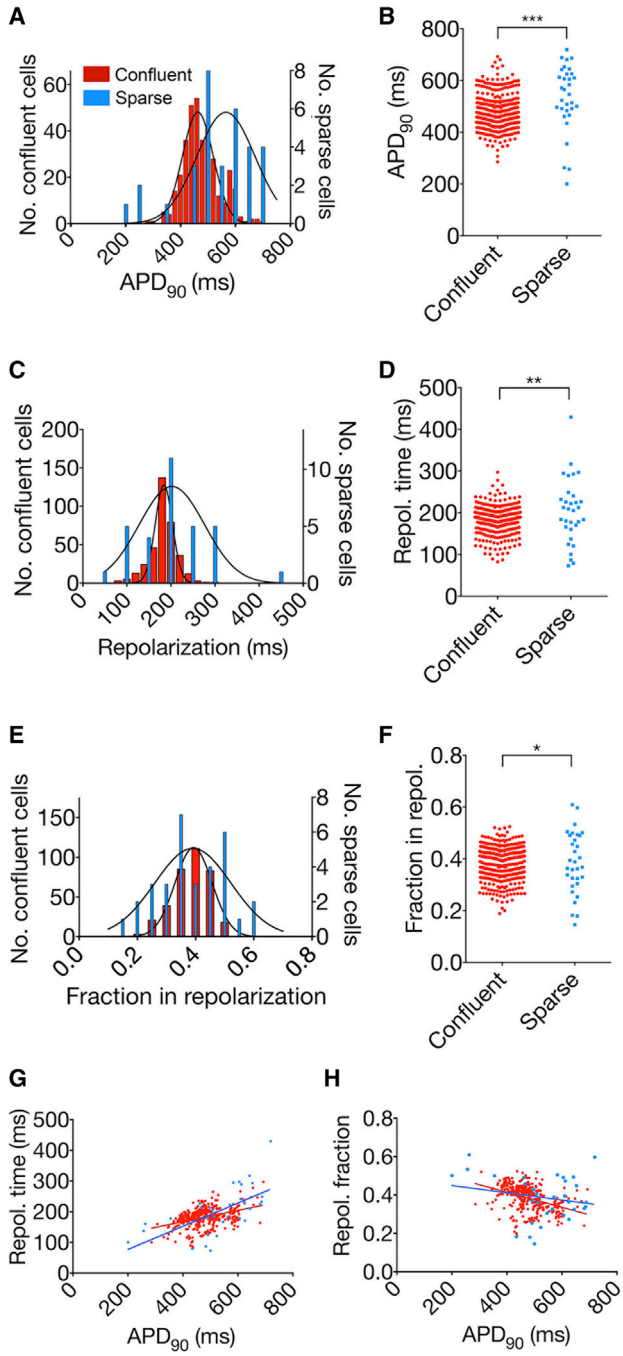

FIGURE 2 (*A*, *C*, and *E*) Distribution of APD_{90}, absolute repolarization time, and AP fraction in repolarization of cells in both seeding groups. Gaussian functions were fitted to binned distributions (*solid lines*). (*B*) Distributions of APD_{90} in the two groups are significantly different ($p < 0.001$). (*D* and *F*) Statistically significant differences are seen in distributions of repolarization time ($p < 0.01$) and repolarization fraction ($p < 0.05$). (*G*) In both groups, as APD_{90} increases, repolarization time is correspondingly longer. Both seeding groups show a low correlation with duration of AP (confluent $R^2 = 0.167$, sparse $R^2 = 0.396$). (*H*) As AP length increases, repolarization fraction is correspondingly smaller. However, this relationship is poor, and is less obvious in sparsely seeded cells (confluent $R^2 = 0.167$, sparse $R^2 = 0.042$).

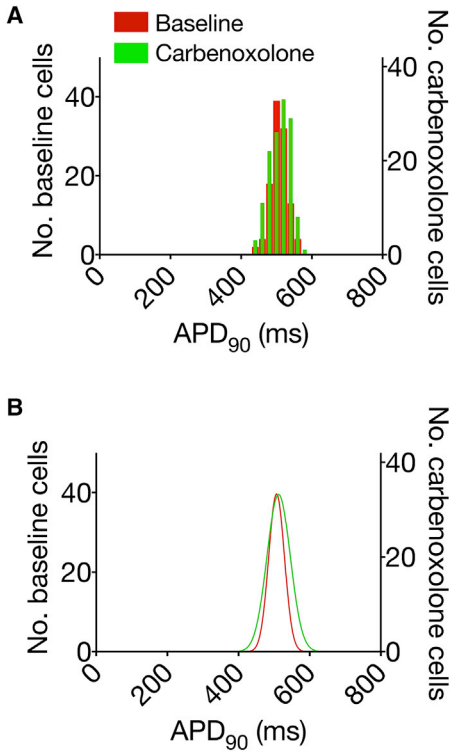

FIGURE 3 The addition of 20 μM carbenoxolone to confluent iPSC-CMs increased variability of APD but only to a limited extent. (*A*) Frequency distribution of APD_{90}. (*B*) Gaussian function fitted to the frequency distributions. Bars have been removed for clarity. Baseline cells, $n = 112$; carbenoxolone cells, $n = 133$.

The AP morphologies of sparsely seeded cells displayed a lower goodness-of-fit, but even in this case there is no clear evidence of chamber-specificity.

These data suggest that iPSC-CMs possess a *sui generis* AP morphology, and when observed in different seeding densities may encompass any shape including those resembling chamber-specific subtypes. Thus, AP morphology of iPSC-CMs does not predict cardiac chamber subpopulations, and contests the now widely-accepted assumption that AP morphology can be used to discriminate these cells on a chamber-specific basis. Further studies characterizing AP morphology from cells in different culture conditions are required in order to fully reveal the potential of iPSC-CMs for applications in tissue regeneration, and as an accurate and robust assay for drug-testing and disease modeling.

Limitations of this study are included in the Supporting Material.

SUPPORTING MATERIAL

Supporting Materials and Methods are available at http://www.biophysj.org/biophysj/supplemental/S0006-3495(14)01191-6.

ACKNOWLEDGMENTS

The authors thank Dr. Patrizia Camelliti for her help in the early stages of these experiments, and Dr. Francis Burton for his support with OPTIQ software.

REFERENCES

1. Bizy, A., G. Guerrero-Serna, …, J. Jalife. 2013. Myosin light chain 2-based selection of human iPSC-derived early ventricular cardiac myocytes. *Stem Cell Res. (Amst.).* 11:1335–1347.
2. Burridge, P. W., S. Thompson, …, E. T. Zambidis. 2011. A universal system for highly efficient cardiac differentiation of human induced pluripotent stem cells that eliminates interline variability. *PLoS ONE.* 6:e18293.
3. Haase, A., R. Olmer, …, U. Martin. 2009. Generation of induced pluripotent stem cells from human cord blood. *Cell Stem Cell.* 5:434–441.
4. Itzhaki, I., L. Maizels, …, L. Gepstein. 2011. Modelling the long QT syndrome with induced pluripotent stem cells. *Nature.* 471:225–229.
5. Ivashchenko, C. Y., G. C. Pipes, …, R. N. Willette. 2013. Human-induced pluripotent stem cell-derived cardiomyocytes exhibit temporal changes in phenotype. *Am. J. Physiol. Heart Circ. Physiol.* 305:H913–H922.
6. Ma, J., L. Guo, …, C. T. January. 2011. High purity human-induced pluripotent stem cell-derived cardiomyocytes: electrophysiological properties of action potentials and ionic currents. *Am. J. Physiol. Heart Circ. Physiol.* 301:H2006–H2017.
7. Moretti, A., M. Bellin, …, K. L. Laugwitz. 2010. Patient-specific induced pluripotent stem-cell models for long-QT syndrome. *N. Engl. J. Med.* 363:1397–1409.
8. Xu, H., B. A. Yi, …, K. R. Chien. 2012. Highly efficient derivation of ventricular cardiomyocytes from induced pluripotent stem cells with a distinct epigenetic signature. *Cell Res.* 22:142–154.
9. Zhang, J., G. F. Wilson, …, T. J. Kamp. 2009. Functional cardiomyocytes derived from human induced pluripotent stem cells. *Circ. Res.* 104:e30–e41.
10. Blazeski, A., R. Zhu, …, L. Tung. 2012. Electrophysiological and contractile function of cardiomyocytes derived from human embryonic stem cells. *Prog. Biophys. Mol. Biol.* 110:178–195.
11. Dhillon, P. S., R. Gray, …, N. S. Peters. 2013. Relationship between gap-junctional conductance and conduction velocity in mammalian myocardium. *Circ. Arrhythm. Electrophysiol.* 6:1208–1214.

Action Potential Morphology of Human Induced Pluripotent Stem Cell-Derived Cardiomyocytes Does Not Predict Cardiac Chamber Specificity and Is Dependent on Cell Density

Supporting Material

David TM Du, Nicola Hellen, Christopher Kane and Cesare MN Terracciano*

Myocardial Function Section, National Heart and Lung Institute, Imperial Centre for Translational and Experimental Medicine, Imperial College London, Du Cane Road, London, W12 0NN, UK

*Correspondence: c.terracciano@imperial.ac.uk

Supplementary information

Methods

Cardiomyocyte preparation

iPSC-CMs (iCell Cardiomyocytes – Cellular Dynamics International, Madison, WI, USA) were plated as per manufacturer's protocol onto 14 mm glass-bottomed dishes (MatTek, USA). iPSC-CMs were plated at two different seeding densities: 60,000 cells/well (confluent monolayer) and 15,000 cells/well (sparsely-seeded). Cells were incubated at 37°C in 5% CO_2 before use 14 days from seeding. Subsequent experiments were performed to assess the effect of gap junction communication in confluently-seeded preparations on action potential morphology. iPSC-CM action potentials were assessed, as below, before and after the application of 20 μM carbenoxolone (Sigma Aldrich) (1).

Imaging

Action potential morphology was assessed using the voltage-sensitive fluorescent dye di-8-ANEPPS (Invitrogen). iPSC-CMs were loaded with 5 μM di-8-ANEPPS in 1 ml DMEM at 37°C for 20 minutes. 4 μM blebbistatin was added 5 minutes before recording to inhibit excitation-contraction coupling and prevent signal distortion due to motion artefact. Di-8-ANEPPS was excited using a 535-nm LED and the emitted fluorescence collected through a 590-nm long-pass filter. The cells were electrically field stimulated at 1 Hz with a 20±10V stimulus of 5 ms duration and five-second recordings were captured using a NeuroCMOS camera (Redshirt) at 1 kHz using a ×40 oil-immersion objective. Dishes were kept at 37°C in normal Tyrode's solution (in mM: 140 NaCl, 4.5 KCl, 10 Glucose, 10 HEPES, 1 $MgSO_4$, 1.8 $CaCl_2$ – pH 7.4) throughout recording. Six dishes were studied in the confluent group, with 2-7 recordings taken per dish. Two dishes were studied for the sparse group, with 1-4 recordings taken per dish. Four dishes were studied for the carbenoxolone experiments, with 5-6 recordings taken per dish.

Image processing

Recordings were captured at 128 × 128 pixels. Individual cardiomyocytes were selected post-hoc in Optiq (Dr Francis Burton, University of Glasgow, Glasgow, UK) using a rectangular selection tool. In confluent monolayer each cardiomyocyte selection had sizes ranging from approximately 10 × 10 – 17 × 17 pixels, corresponding to approximately 31.25 × 31.25 – 53.125 × 53.125 μm. In sparsely seeded dishes, each cardiomyocyte selected had a size ranging from approximately 25 × 25 – 56 × 56 pixels, corresponding to 78.125 × 78.125 – 175 × 175 μm. Sparse cells were in partial contact with each other. AP analysis software, Optiq, was used for selection of cardiomyocytes and for curve fitting and automated measurement of AP parameters: amplitude, time to peak, APD_{90}, and APD_{50} (Fig. 1, A, B and C). Repolarization was measured with respect to the maximum diastolic potential of each

AP. Parameter measurements from three consecutive APs per cardiomyocyte were recorded and averaged for analysis. iPSC-CMs that could not be paced at 1 Hz were not assessed.

Statistical analysis

Statistical analysis of APD_{90} and repolarization was performed using Prism6 (GraphPad Software Inc., San Diego, CA, USA) and parametric tests of variance (F-test) were performed using MedCalc 14.8.1 (MedCalc Software bvba, Ostend, Belgium). The non-parametric two-tailed unpaired Kolmogorov-Smirnov (K-S) test was used to determine statistical differences in distribution. Student's *t*-test with Welch's correction was used to determine differences in mean APD in the carbenoxolone experiments. $P<0.05$ was considered statistically significant. Data are expressed as mean (SD). n signifies the number of cardiomyocytes analyzed. No assumptions were made with respect to the distribution of the populations. Parametric and non-parametric tests were performed due to the relatively low number of sparse cells producing equivocal distributions.

Limitations

(1) The use of blebbistatin for inhibition of mechanical function. However, there is conflicting evidence as to whether or not blebbistatin affects APD (2, 3). Both of these reports used Langendorff-perfused whole hearts to optically measure APD; whether APD prolongation is due to myocytes being mechanically unloaded, or is a direct effect of blebbistatin on the cardiomyocyte, however, cannot be established.

(2) The use of a single source of iPSC-CMs; future studies will test iPSC-CMs from different manufacturers using different culture mediums and culture times.

References for supporting material:

(1) Dhillon, P. S., Gray, R., Kojodjojo, P., Jabr, R., Chowdhury, R., Fry, C. H., & Peters, N. S. (2013). Relationship between gap-junctional conductance and conduction velocity in mammalian myocardium. Circulation. Arrhythmia and Electrophysiology, 6(6), 1208–14

(2) Brack, K.E., R. Narang, J. Winter, and G.A. Ng. (2013). The mechanical uncoupler blebbistatin is associated with significant electrophysiological effects in the isolated rabbit heart. Exp. Physiol. 98: 1009–27

(3) Fedorov, V. V, Lozinsky, I. T., Sosunov, E. a, Anyukhovsky, E. P., Rosen, M. R., Balke, C. W., & Efimov, I. R. (2007). Application of blebbistatin as an excitation contraction uncoupler for electrophysiologic study of rat and rabbit hearts. Heart Rhythm : The Official Journal of the Heart Rhythm Society, 4(5), 619–26